



HAL
open science

Mechanical coupling through the skin affects whisker movements and tactile information encoding

Valerie Ego-Stengel, Aamir Abbasi, Margot Larroche, Henri Lassagne, Yves Boubenec, Daniel Shulz

► **To cite this version:**

Valerie Ego-Stengel, Aamir Abbasi, Margot Larroche, Henri Lassagne, Yves Boubenec, et al.. Mechanical coupling through the skin affects whisker movements and tactile information encoding. *Journal of Neurophysiology*, 2019, 122 (4), pp.1606 - 1622. 10.1152/jn.00863.2018 . hal-04005103

HAL Id: hal-04005103

<https://hal.science/hal-04005103>

Submitted on 7 Mar 2023

HAL is a multi-disciplinary open access archive for the deposit and dissemination of scientific research documents, whether they are published or not. The documents may come from teaching and research institutions in France or abroad, or from public or private research centers.

L'archive ouverte pluridisciplinaire **HAL**, est destinée au dépôt et à la diffusion de documents scientifiques de niveau recherche, publiés ou non, émanant des établissements d'enseignement et de recherche français ou étrangers, des laboratoires publics ou privés.

1 **Mechanical coupling through the skin affects whisker movements and tactile information**
2 **encoding**

3 **Valerie Ego-Stengel, Aamir Abbasi, Margot Larroche, Henri Lassagne, Yves Boubenec and Daniel**
4 **E. Shulz**

5 Department for Integrative and Computational Neuroscience (ICN), NeuroPSI, CNRS, 91190 Gif-
6 sur-Yvette, France

7

8 *Abbreviated title: Cross-whisker mechanical coupling*

9

10 *Corresponding Authors:*

11 Valerie Ego-Stengel and Daniel E. Shulz

12 Department for Integrative and Computational Neuroscience (ICN)

13 Paris-Saclay Institute of Neuroscience (NeuroPSI)

14 UMR9197 CNRS/University Paris Sud

15 CNRS, Building 32/33, 1 avenue de la Terrasse, 91190 Gif-sur-Yvette, France

16 valerie.stengel@unic.cnrs-gif.fr, daniel.shulz@unic.cnrs-gif.fr

17

18 *Number of pages of the text: 51*

19

20 *Number of figures: 7*

21

22 *Number of words in Abstract: 250*

23

24 *Acknowledgments:*

25

26 We thank the Human Frontier Science Program Organization (CDA 00044-2010), ANR Neurowhisk,

27 Labelled Team FRM DEQ20170336761, Lidex iCODE and NeuroSaclay in the IDEX Paris-Saclay ANR-

28 11-IDEX-0003-02. We thank Camila Pulido and David Davila for their contribution to early whisker
29 tracking and electrophysiology experiments. We are grateful to the whole Shulz lab for advice
30 throughout the project, to Evan Harrell for comments on the manuscript, and to Yannick Passarelli
31 with help finalizing the submission. We thank Guillaume Hucher for measuring whisker
32 parameters and for trigeminal ganglion histology, and Aurélie Daret for help with animal
33 experiments and general lab managing. The authors declare no competing financial interests.
34 Present address of Yves Boubenec: LSP, DEC, Ecole Normale Supérieure, 29 rue d'Ulm, 75005 Paris,
35 France

36 **ABSTRACT**

37 Rats use their whiskers to extract sensory information from their environment. While exploring,
38 they analyze peripheral stimuli distributed over several whiskers. Previous studies have reported
39 cross-whisker integration of information at several levels of the neuronal pathways from whisker
40 follicles to the somatosensory cortex. Here, we have investigated the possible coupling between
41 whiskers at a preneuronal level, transmitted by the skin and muscles between follicles. First, we
42 have quantified the movement induced on one whisker by deflecting another whisker. Our results
43 show significant mechanical coupling, predominantly when a given whisker's caudal neighbor in
44 the same row is deflected. The magnitude of the effect was correlated with the diameter of the
45 deflected whisker. In addition to changes in whisker angle, we observed curvature changes when
46 the whisker shaft was constrained distally from the base. Second, we found that trigeminal
47 ganglion neurons innervating a given whisker follicle fire action potentials in response to high-
48 magnitude deflections of an adjacent whisker. This functional coupling also shows a bias towards
49 the caudal neighbor located in the same row. Finally, we designed a two-whisker biomechanical
50 model to investigate transmission of forces across follicles. Analysis of the whisker-follicle contact
51 forces suggests that activation of mechanoreceptors in the ring sinus region could account for our
52 electrophysiological results. The model can fully explain the observed caudal bias by the gradient
53 in whisker diameter, with possible contribution of the intrinsic muscles connecting follicles.
54 Overall, our study demonstrates the functional relevance of mechanical coupling on early
55 information processing in the whisker system.

56

57 **NEW & NOTEWORTHY**

58 Rodents explore their environment actively by touching objects with their whiskers. A major
59 challenge is to understand how sensory inputs from different whiskers are merged together to
60 form a coherent tactile percept. Here, we demonstrate that external sensory events on one
61 whisker can influence the position of another whisker and, importantly, they can trigger the
62 activity of mechanoreceptors at its base. This cross-whisker interaction occurs pre-neuronally,
63 through mechanical transmission of forces in the skin.

64 INTRODUCTION

65 Rodents navigate and perform challenging tactile discriminations by touching surfaces and objects
66 with their whiskers. The whisker system of the rat consists of approximately 30 whiskers on each
67 side of the snout, which are arranged in a grid-like pattern. This striking discrete peripheral pattern
68 is matched by the anatomical organization of upstream neuronal circuits in grid-like arrays of
69 distinct substructures, called barrelettes, barreloids and barrels in the brainstem, thalamus and
70 cortex respectively (Woolsey and Van der Loos, 1970; Van der Loos, 1976; Ma and Woolsey, 1984).
71 As a first-order description, sensory information travels in parallel pathways or “labelled lines”
72 from each whisker to each cortical barrel (Deschênes and Urbain, 2009).

73 However, already in some of the first recordings in barrel cortex, neurons were shown to exhibit
74 responses to the individual deflection of several whiskers, demonstrating anatomical and
75 functional convergence (Axelrad et al., 1976; Simons, 1978). From a behavioral point of view, the
76 analysis of information coming from several whiskers is indeed important for the animal to
77 perform subtle discrimination tasks (Carvell and Simons, 1995; Krupa et al., 2001; Knutsen et al.,
78 2006). In fact, the complex patterns of whisker movements and contact characteristics are only
79 beginning to be described in detail (Grant et al., 2009; Hobbs et al., 2015; Sherman et al., 2017). A
80 major challenge will be to understand how multiple whisker inputs are merged together to form a
81 coherent tactile percept. Despite already a large number of studies aimed at deciphering the
82 mechanisms of multi-whisker integration, the anatomical and functional circuitry responsible for
83 properties of cortical and thalamic receptive fields remains poorly understood.

84 At the most peripheral level, encoding of tactile stimuli is performed by several classes of
85 mechanoreceptors located in the follicles at the base of the whiskers (Ebara et al., 2002; Ebara et
86 al., 2017). Approximately 150-200 first-order neurons from the trigeminal ganglion (TG) innervate

87 each follicle (Vincent, 1913) in an exclusive manner, that is, one TG neuron innervating only one
88 follicle. This has been originally inferred from functional studies, which all reported that TG
89 receptive fields contain a single whisker (Zucker and Welker, 1969; Gottschaldt et al., 1973; Dykes,
90 1975; Gibson and Welker, 1983). It has been finally confirmed by anatomical means very recently
91 (Tonomura et al., 2015).

92 Upstream, cross-whisker connections have been found among brainstem nuclei (Jacquin et al.,
93 1990; Voisin et al., 2002) and in the thalamo-cortico-thalamic loop (Arnold et al., 2001; Lavallée
94 and Deschênes, 2004). They are especially numerous intracortically (Bernardo et al., 1990;
95 Narayanan et al., 2015), where they constitute a potential substrate for multiple forms of multi-
96 whisker sensory integration (reviewed in Estebanez et al., 2017).

97 Nonetheless, there remains another possibility for early generation of cross-whisker signals,
98 namely that external contact forces on one whisker could lead to activation of mechanoreceptors
99 in a neighbor follicle. Indeed, in the whisker system, sensory contacts occur on the shaft of the
100 whisker, up to several centimeters away from the receptors in the follicle. Pre-neuronal treatment
101 by the whisker itself transforms the dynamics of contact into a time course of forces at the base of
102 the whisker (Boubenec et al., 2012; Boubenec et al., 2014; Quist and Hartmann, 2012; Bagdasarian
103 et al., 2013). How these forces then translate into mechanoreceptor activation has just started to
104 be studied (Whiteley et al., 2015). Interestingly, the possibility of cross-whisker mechanical
105 coupling has been suggested more than thirty years ago following the report of one TG neuron
106 activated by a second whisker beyond its principal whisker (Simons, 1985, Figure 4). This study
107 suggested the existence of “mechanical spread of the stimulus energy through the mystacial pad”.
108 Indeed, follicles are embedded in a complex mesh composed of skin, conjunctive tissue, and
109 several muscles (Dörfl, 1982; Haidarliu et al., 2010). Extrinsic muscles both for retraction
110 (nasolabialis and maxillolabialis muscles) and protraction (nasalis muscle) run superficially,

111 associated closely with the corium in the skin. Intrinsic muscles connect the top of each follicle
112 with the deep part of its rostral neighbor. Interactions between follicles may be transmitted
113 through the superficial layer of skin and/or via these different muscles.

114 We have developed two experimental approaches to study cross-whisker interactions. First, we
115 have imaged individual whiskers using high resolution videography of the snout of anesthetized
116 rats while deflecting whiskers with high precision (Jacob et al., 2010). We quantified the
117 deformation of a non-deflected whisker while another whisker was moved in terms of
118 displacement, angle and curvature. Second, we performed electrophysiological recordings of
119 individual TG neurons. We investigated whether mechanical coupling can be sufficient to induce
120 spikes in trigeminal neurons without stimulating their principal whisker. We integrate our results
121 in a two-whisker biomechanical model bridging the gap between the external profile of the
122 whisker on the one hand, and the internal distribution of forces on the other hand, ultimately
123 responsible for mechanoreceptor activation.

124

125 **MATERIALS AND METHODS**

126 ***Animal preparation***

127 All experiments were performed in conformity with French (Decree 2013-118, Ethics Committee
128 project #3249-2015060516116339) and European (2010/63/EU) legislation on animal
129 experimentation. Thirteen male Wistar rats (weight 250-300g) were used in this study. Animals
130 were housed in the NeuroPSI animal facility on a 12:12 light schedule, with 2-4 animals per cage.
131 The animals were handled regularly and fed ad libitum. The experiment was always conducted
132 during the light phase of the cycle. A group of 7 rats was used for videography experiments and
133 another group of 6 rats was used for electrophysiology experiments. Atropine methyl nitrate
134 (0.3mg/kg im) was injected to reduce secretions in the respiratory path. Rats were anesthetized
135 with urethane (1.5 g/kg ip). The level of anesthesia was monitored by observing the absence of
136 eye blink reflex, the lack of response to hind paw pinch, and the absence of spontaneous whisker
137 movements. Supplementary doses of urethane (0.15 g/kg ip) were administered whenever
138 necessary throughout the experiment in order to maintain an adequate level of anesthesia. Body
139 temperature was maintained at 37°C by a regulated heating pad. The animal was placed in a
140 stereotaxic frame. The snout was held by a modified head holder (Haidarliu, 1996) allowing free
141 access to the right whisker pad. A local anesthetic (Lidocaine 1%) was injected subcutaneously and
142 the skin on top of the skull was resected. After cleaning the conjunctive tissues, the skull was
143 cemented to a metal bar fixed rigidly to the frame. This allowed us to remove the right ear bar,
144 and to position the multi-whisker stimulator near the right whisker pad.

145

146 ***Whisker stimulation***

147 We used a custom-made whisker stimulation matrix based on piezoelectric benders (Jacob et al.,

148 2010) to deflect independently the 24 most caudal whiskers of the right whisker pad. Whiskers
149 were trimmed to 10-mm length in order to avoid unwanted deflections due to whisker tips
150 accidentally touching neighboring stimulators. Whiskers were inserted 3 mm into small
151 polypropylene tubes glued on each bender (Polytec-PI), thus stimulated at 7 mm from their base.
152 Benders were driven with RC-filtered voltage pulses producing a trapezoidal deflection. Our
153 standard parameters produced pulses of 10 ms ramp, 10 ms plateau, and 10 ms ramp back, with
154 an amplitude of 1° applied at 7 mm from the follicle, either in a rostral or a caudal direction. We
155 checked that the movement always stayed within +/- 10% of its expected value by laser
156 measurement.

157

158 ***Videography experiments***

159 *High-speed high-resolution video recording*

160 A high-speed camera (Photron Fastcam SA3/105mm f-2.8 DG Macro Sigma) was mounted
161 vertically above the animal to record the whisker movements at a 1 kHz frame rate. The camera
162 was triggered by a TTL sent by the whisker stimulator. Whiskers were illuminated from below
163 using a backlight (SSLUB, Phlox and PP520, Gardasoft). The camera was initially positioned to give
164 a bird's-eye view of the C2 whisker, and later translated above other whiskers. Given the
165 geometrical constraints of the multiwhisker stimulator and the camera, we could only move the
166 whiskers in a rostro-caudal direction and image them from the top. For calibration of the spatial
167 scale of the camera field, we imaged a standard checkerboard sheet (1mm x 1mm). Pixel
168 resolution was checked for each series of movies and was in the range 16-20 µm.

169

170 *Whisker stimulation protocols*

171 To study the effects of mechanical coupling across the whisker pad, we first imaged whisker C2

172 while deflecting each of the other 23 whiskers individually. For each deflected whisker, we
173 performed 4 trials in the caudal direction and 4 trials in the rostral direction. Non-stimulated
174 whiskers were let free in air (not inside the stimulator tips). The whole protocol was first applied
175 while the imaged whisker C2 itself was free in air ("Free" condition). Then, the protocol was
176 repeated (in 4 experiments out of 7) while constraining whisker C2 in its corresponding stimulator
177 tip without movement ("Constrained" condition).

178 In 3 experiments out of 7, we tested mechanical coupling effects on other whiskers in addition to
179 whisker C2. Given the camera angle and snout geometry, we were able to image whiskers located
180 in rows B to D and arcs 1 to 3. Overall, we imaged 21 additional whiskers while deflecting either
181 the immediately caudal or the immediately rostral adjacent whisker. Those tests were
182 systematically done both in "Free" and "Constrained" conditions. For Arc 1 whiskers, we chose to
183 test their coupling on the caudal side with the straddler resulting in the smoothest alignment of
184 follicles (B1-Beta, C1-Gamma, D1-Delta), which correlates with the presence of an intrinsic muscle
185 (Haidarliu et al., 2010).

186

187 *Measurement of whisker parameters*

188 At the end of the experiment, after all movies were acquired, we estimated the point of the
189 whisker shaft corresponding to follicle entry for each imaged whisker. First, a wide-field snapshot
190 of all whiskers and of the snout fur was taken. Then, we spread depilatory cream on the fur
191 between the whiskers, let it set for 3-5 min, and carefully removed the cream and rinsed the pad.
192 We took a second wide-field snapshot of the whisker pad without the fur, adjusting the lighting so
193 that the entry of the whiskers in their follicles were clearly visible. Finally, whiskers were cut at the
194 follicle entry and mounted on histology slides for measurement of their diameter and length under
195 an optical microscope. For the D row, which was located below the pad outline and/or below

196 other whiskers, the follicle entry position could often not be directly visualized. In those instances,
197 it was estimated on the wide-field snapshot using the visible tip and the known length of the
198 whisker, and taking into account the angle of the whisker relative to the horizontal plane of focus.

199

200 *Data analysis*

201 Camera recordings were analyzed using custom scripts in python. Each movie contained 150 or
202 200 frames at 1 kHz, corresponding to one trial. Frames were typically 384 * 512 pixels. Their exact
203 dimension was adjusted from one imaged whisker to the next depending on the viewing
204 conditions. A series of eight trials (4 rostral, 4 caudal deflections) was analyzed for each pair of
205 imaged and moved whiskers, and for each “Free” and “Constrained” conditions tested.

206 In all movies, the imaged whisker was approximately vertical on each frame, with the fur visible at
207 the bottom (Figure 1A). We defined a range of pixel lines in which the imaged whisker appeared
208 clearly as a dark bar on a lighter background. For each line, the center of the whisker shaft was
209 defined as the center of mass of the pixels encompassing the whole section of the whisker on that
210 line (usually about 15 pixels), where each pixel is weighed by its intensity value compared to a
211 given threshold. The threshold was adjusted independently for each imaged whisker. This yielded
212 a raw profile of the whisker corresponding to the current frame (such as one colored line in Figure
213 1). The computation was applied independently to each frame. We systematically checked whisker
214 tracking for each movie, by plotting several calculated raw profiles on top of their corresponding
215 images. This allowed to correct tracking problems due to unexpected changes (background
216 element, global shift) mainly by changing the threshold or modifying the range of lines tracked.

217 Raw profiles of whiskers were never smooth, displaying many irregularities. Subpixel high-
218 frequency spatial oscillations, dependent on the initial angle of the whisker relative to the vertical
219 axis of the frames, could be ascribed to pixelization artifacts by the camera and were ignored in

220 our analysis. We also encountered enlarged portions of a shaft, particles sticking on it, or bends.
221 To focus on the changes over time irrespective of these singularities, we subtracted the profile
222 calculated on the frame just before the start of the stimulation from all other profiles of the
223 movie. We characterized the resulting deformation profiles, as well as the reference raw profile,
224 by fitting each of them with a second-degree polynomial. This allowed us to extract three
225 parameters quantifying the deformation: the displacement along the rostro-caudal axis, the
226 change in whisker angle, and the change in curvature. These three parameters could be estimated
227 at any point along the whisker shaft.

228 The tracked portion of the whisker was limited by the imaging constraints, in particular on the
229 follicle side for which the view was obstructed by other whiskers and fur. We extrapolated the fits
230 of the whisker profiles down to the estimated follicle entry. For population analysis, we filtered
231 out trials for which the displacement near the tip or the change in angle near the follicle were
232 outside of the range: mean \pm 1.5 * sd, either in the baseline window 20 to 10 ms before the start
233 of stimulation, or in a second baseline window 10 to 20 ms after the end of stimulation. This
234 eliminated 5-15% of trials on one given experiment, depending on the stability of the preparation.

235 To validate our method, in one animal we tracked the kinematic changes of whisker C1 while it
236 was being deflected by its piezoelectric bender (Figure 1A-D). For each frame, a weighted average
237 of pixel intensities across the whisker was performed line by line, in the region where the contrast
238 of the whisker against the background was sufficiently good. The left side of Figure 1B shows the
239 expanded resulting profiles of whisker C1 for 20 frames, corresponding to 20 ms during its
240 deflection by the stimulator. The whisker tip was indeed deflected by the expected amount (114
241 μ m, i.e. about 7 pixels). Meanwhile, the whisker shaft showed a change in angle, which was largest
242 towards the base of the whisker, as well as an increase in curvature which was best seen when
243 looking at the deformation relative to rest (Figure 1C Left). We fitted each profile independently

244 by a second-order polynomial as described above. The fits (gray lines on Figure 1B-C) were
245 extrapolated down to the estimated follicle entry point. Overall, the C1 imposed deformation
246 appears as a rotation of the whisker around the follicle entry point with a change in curvature. We
247 quantified several kinematic parameters at each point along the shaft: displacement in the rostro-
248 caudal direction, angle relative to rest, and curvature. Figure 1D displays the evolution of these
249 parameters in time for the tip, middle and follicle entry points. Note that residual ringing can be
250 observed after ramp deflections, typical of piezoelectric stimulation (Jacob et al., 2010). Overall,
251 these measures on the deflection of C1 confirm that our imaging method can measure sub-pixel
252 deformations of a whisker at a 1kHz resolution.

253 We report median and interquartile range values. We performed non-parametric statistical tests
254 because of low sample sizes. Individual tests are referred to in the main text.

255

256 ***Electrophysiology experiments***

257 *Signal acquisition and spike sorting*

258 In addition to the surgical steps for head fixation, a craniotomy was made on the skull overlaying
259 the right trigeminal ganglion (P-1.8, L-2.1 from bregma; Schneider et al., 1981). A dam of dental
260 acrylic was constructed around the craniotomy and filled with saline to prevent the brain from
261 drying. Extracellular neural activity was recorded from a tungsten electrode (FHC 2-10 M Ω at 1
262 kHz) that was vertically lowered about 10 mm down in the TG using an electronically controlled
263 manipulator (Luigs and Neumann). Custom-made software (Elphy, G. Sadoc, UNIC, CNRS) was used
264 for spike time acquisition, whisker stimulation, and data processing. In a first series of experiments
265 (5 cells in 2 rats), signals were amplified and filtered (300-3000Hz) by an acquisition card
266 (CyberAmp) connected to a template-matching hardware spike sorter (Alpha-Omega). In a second
267 series (9 cells in 4 rats), signals were amplified and filtered (250-7500Hz) using a different

268 acquisition system (Blackrock Microsystems, USA). Single units were isolated using the integrated
269 online spike sorter. In all experiments, baseline signals had a standard deviation of 10-15 μV .
270 Single-unit spike waveforms had amplitudes of 100 μV or more. Because cell density and cell firing
271 are sparse in the trigeminal ganglion, we typically recorded at most one or a few action potentials
272 per stimulus separated by long periods of silence. Thus, action potential waveforms were clearly
273 separated from the noise. The shape of action potentials was closely monitored online to ensure
274 that only isolated single-units were recorded throughout the protocols. The recording was
275 terminated if the quality of spike classification was lost. At the end of recording at a given site, the
276 electrode was advanced by at least 100 μm before the next recording site to avoid recording data
277 from the same single units.

278

279 *Whisker stimulation protocols*

280 We first characterized the receptive field of each neuron by presenting pseudo-random sequences
281 of 30 to 100 individual deflections of the 24 whiskers in the rostral and caudal directions. Initially,
282 we applied pulses of 0.93° (2 experiments) or 1° (4 experiments), corresponding to angular speeds
283 of $93\text{-}100^\circ/\text{s}$. Once the receptive field of the neuron was established, we tested mechanical
284 coupling across an increasing range of ramp speeds. We increased the deflection amplitude to 3°
285 or 4° , resulting in an increase in ramp speed to $300^\circ/\text{s}$ or $400^\circ/\text{s}$ respectively. We also reduced the
286 ramp duration from 10 ms to 5 or 3 ms, to increase the deflection speed up to $1,200^\circ/\text{s}$. In a few
287 cases, we approached further the stimulator tip along adjacent whiskers down to about 3 mm
288 from the follicle, which resulted in an increased speed of the deflection to about $4,000^\circ/\text{s}$. These
289 different parameter modifications were tested until a coupling effect was observed from one
290 adjacent whisker, at which point we stopped increasing ramp speed. Interestingly, all neurons for
291 which we were able to test this range of increasing ramp speeds displayed mechanical coupling

292 effects for at least one adjacent whisker. For other neurons, the quality of single-unit isolation was
293 lost before high speeds could be tested.

294 Beyond a direct response of a primary afferent neuron to one of the adjacent whiskers, we tested
295 whether a movement of an adjacent whisker could modify the response of the neuron to
296 deflections of its principal whisker, through a subthreshold modulation. We first determined
297 deflection parameters for the coupled adjacent whisker which elicited no response for either
298 direction of movement. We then stimulated the principal whisker in its preferred direction with
299 eight different pulses of increasing speed and fixed amplitude stimuli, obtaining a response curve
300 as a function of speed. Once all parameters were determined, we studied the modulation of this
301 curve by adding subthreshold deflections to the adjacent whisker in either direction. Trials with
302 only the principal whisker deflected, or with deflections of both the principal whisker and the
303 adjacent whisker in either rostral or caudal direction, were pseudo-randomly interleaved. We
304 could only complete this final protocol satisfactorily in one case (Figure 6).

305

306 *Data analysis*

307 Peri-stimulus time histograms (PSTHs) were constructed by summing the activity of the neuron
308 relative to the stimulus trigger with a 1-ms time bin. Spontaneous activity was null for 13 out of 14
309 neurons, and below 1 Hz for the remaining neuron.

310

311 ***Biomechanical model***

312 A finite-element model of two whiskers and follicles was built in SolidWorks Simulation.
313 Geometrical parameters such as whisker diameter, follicle dimensions and inter-whisker spacing
314 are known to vary across the whisker pad. We used values obtained from the literature (Kim et al.,
315 2011; Haidarliu et al., 2010) and complemented from our own measurements taken in the center

316 of the whisker pad on and around C2. Note that the chosen geometry needed to be compatible
317 with a mesh model, thus avoiding very small features and very high curvature surfaces. This forced
318 us in particular to use a larger whisker diameter than typical values for the rat. Hence, each
319 whisker was modelled by a rod of diameter 300 μm , i.e. twice thicker than the C2 whisker of our
320 animals (149 μm , $n = 4$ rats; see also Belli et al., 2017). To investigate the impact of whisker
321 diameter on the forces inside the follicle, we also tested diameters of 250 and 350 μm (see
322 Results). The whisker rod was 10 mm long, modelling a cut whisker of which the tip would be
323 manipulated. Each follicle was modelled by a cylinder of diameter 800 μm and length 2.5 mm in
324 which a whisker was inserted. Follicle centers were 2 mm apart. Follicles and whiskers were
325 attached at their base to a fixed plate. A layer of skin was added in which the top of the follicles
326 was embedded. This rectangular skin component had a thickness of 80 μm and extended 750 μm
327 in each direction from the follicle borders. We did not attempt to model the extrinsic muscles
328 running along the corium separately, but considered the skin sheet as including those muscles. For
329 one set of simulations, we modelled the intrinsic muscle as a single rod connecting two rings, one
330 around the caudal follicle just below the skin, and one around the rostral follicle centered at a
331 depth of two thirds of the total follicle depth. The ring was 200 μm thick and 300 μm high. The
332 connecting rod had a diameter of 100 μm .

333 Follicles and skin, as well as the intrinsic muscle when simulations included one, were modelled by
334 a material with mechanical parameters close to Rubber with Young's modulus = 0.12 GPa and
335 Poisson's ratio = 0.49. Whiskers were modelled by a material close to PVC with Young's modulus =
336 7.2 GPa, in agreement with measures present in the literature (Hartmann et al., 2003; Neimark et
337 al., 2003; Carl et al., 2012), and Poisson's ratio = 0.38.

338 The contact surfaces between components did not allow penetration. Follicles and skin, as well as
339 the intrinsic muscle when present, were bonded, whereas follicles and whiskers could separate.

340 The mesh size was 80 μm , which resulted in 51,567 elements and 83,978 nodes for our default
341 geometrical parameters. Whisker deflection was modelled by a rotation of the whisker tip of 1°
342 around the whisker base center at the bottom of the follicle. The neighboring whisker distal tip
343 could be either "Free" or "Constrained" (fixed). These boundary conditions on the deflected
344 whisker and its neighbor imposed the whisker angles at the distal end, which was not the case in
345 the experimental conditions. The distal whisker profiles could thus sometimes differ from the
346 observed ones. This did not affect deformations near and inside the follicles, which were the focus
347 of our study.

348 Simulations were run for both rostral and caudal directions of movement. Because results were
349 always found to be symmetric, we chose to report the effect of deflecting one whisker towards
350 the other. Thus, the Rostral whisker was deflected caudally, and the Caudal whisker was deflected
351 rostrally. The simulations all assumed a linear elastic behavior of the components and were
352 restricted to small displacements.

353 **RESULTS**

354 ***High-speed videography reveals whisker movements induced by mechanical coupling***

355 We investigated mechanical coupling between whiskers by imaging directly the whiskers on the
356 snout of rats (n = 7) using a high-frame-rate high-resolution camera and a custom-built multi-
357 whisker stimulator (Jacob et al., 2010).

358 First, we validated our tracking method by verifying that the movement of a whisker deflected by
359 a piezoelectric bender could be imaged at 1 kHz and quantified with adequate spatial resolution
360 (Figures 1A-D, whisker C1, see Methods). We then applied this tracking method to the neighboring
361 whisker C2. As shown by the raw profiles and fits in Figure 1B, whisker C2 also moved during the
362 deflection of whisker C1, even though it was not directly deflected by the experimenter. Moving
363 whisker C1 induced a displacement at the tip of C2 of 25 μm , representing 23% of the tip
364 displacement imposed on C1. For both the deflected and the imaged whisker, there was little if
365 any translation at the base of the whisker, as estimated by extrapolating the whisker profile down
366 to the follicle entry point. The change in angle along whisker C2 reached 0.16°, that is, 11% of the
367 imposed angle at the C1 follicle entry. There was no change in curvature of whisker C2, so that the
368 overall deformation was well described by a change in angle (Figure 1C-D, right). These results
369 demonstrate that even for small movements, there can be a measurable mechanical coupling
370 between two neighboring whiskers. Deflection of one whisker induced a rigid transformation of its
371 rostral neighbor, more precisely a rotation around the follicle entry point.

372

373 ***Mechanical coupling is strongest from a caudal whisker in the same row***

374 We explored the effect of deflecting one by one each whisker, always measuring the movement of
375 the non-deflected central whisker C2. The time course of the angular rotation of C2 for all trials of

376 one experiment is shown on Figure 2A, separately for deflections in the caudal (left panel) and
377 rostral (right panel) directions. For each given deflected whisker, the observed profile was highly
378 repeatable from one trial to the next. In this example, we observed mechanical coupling for
379 deflections of whiskers Beta, B1, Gamma, C1 and C3. The effect was similar for deflections in the
380 caudal and rostral directions, showing mirroring profiles. We thus pooled induced effects across
381 the two conditions for all subsequent population analysis and figures. Analysis from seven
382 experiments confirmed a consistent gradient of the amplitude of induced movement of C2 while
383 moving other whiskers around it (Figure 2B). As observed in Figure 1, induced movements were
384 rigid rotations along the estimated follicle entry, with no curvature change or translation at the
385 base of the whisker. For further analysis, we thus focused on changes in whisker angles (middle
386 matrix of Figure 2B). The effect tended to decrease as the distance between C2 and the deflected
387 whisker increased. However, distance was clearly not the only factor determining the amplitude of
388 the mechanical coupling. We observed a strong asymmetry among whiskers, with whiskers caudal
389 to C2 generating much larger induced movements than those located rostrally. Also, whiskers in
390 the same row as C2 were more effective, suggesting an effect more potent along rows than along
391 arcs.

392

393 ***The strength of mechanical coupling depends on whisker location***

394 Given that not all whisker pairs exhibited detectable mechanical coupling, we wondered which
395 parameters govern the amplitude of the coupling effect. Figure 2B suggests that distance between
396 the whiskers is an important factor, as well as location in the same row. Also, it points to an
397 asymmetry depending on whether the deflected whisker is located rostrally or caudally to the
398 imaged whisker. However, these results were obtained by always imaging C2, so that the
399 asymmetry could also be due to the identity of the whisker moved and not to its rostral vs. caudal

400 location relative to the imaged whisker.

401 We decided to investigate this question further by testing other combinations of whiskers
402 distributed across the whisker pad. We focused on immediately neighboring pairs in one row, for
403 which the effect was expected to be largest, and for which the distance between the follicles is
404 always around 2 mm. The results of this dataset are summarized in Figure 3. First, we checked
405 whether the asymmetry observed for whisker C2 in Figure 2 held when analyzing results from all
406 whiskers imaged, located in rows B-D and arcs 1-3. Indeed, the coupling effect was consistently
407 strongest when the whisker immediately caudal was deflected, compared to the rostral one
408 (Figure 3A, Wilcoxon signed-rank test, $P = 1.2 \cdot 10^{-5}$). In this same dataset, we could also ask
409 whether for a particular combination of whiskers, the effect was similar whichever whisker was
410 the deflected one. We found again that induced movements were larger when deflecting the
411 caudal whisker, compared to the rostral whisker (Figure 3B, Wilcoxon signed-rank test, $P =$
412 0.0023). Moreover, when we compared the impact of deflecting a fixed whisker on its two
413 immediate neighbors, we found that the effect was strongest on the rostral whisker compared to
414 the caudal one, in each of the five cases where we could image on both sides (Figure 3C, Wilcoxon
415 signed-rank test, $P = 0.043$). Together, these results point to a consistent underlying asymmetry,
416 such that mechanical coupling is strongest when the whisker inducing the movement of its
417 neighbor is located caudally to it. Pooling results from all experiments, we looked at whether there
418 was a systematic bias due to the location of the whiskers on the whisker pad (Figure 3D). We
419 observed strong variations in the coupling amplitude across the whisker pad, with larger effects in
420 more caudal and ventral locations.

421 We reasoned that this spatial distribution must arise from a systematic gradient in one or several
422 mechanical parameters across the whisker pad. Many such gradients have been reported and all
423 of them follow a set of consistent rules. In particular, from rostro-dorsal to caudo-ventral

424 locations, the whisker diameter increases sharply (Ibrahim and Wright 1975; Voges et al., 2012;
425 Belli et al., 2017), along with a moderate increase in follicle size and distance between follicles
426 (Haidarliu et al., 2010; also observed in our sample). Because the thickness of the deflected
427 whisker directly governs its mechanical rigidity, it could have a strong impact on the surrounding
428 skin, including neighboring follicles and whiskers. We thus examined the relation between the
429 diameter of the whiskers, measured in 4 animals, and the amplitude of the coupling effect.
430 Median diameters are indicated on Figure 3D by the size of the gray circles and, as expected, co-
431 varied with the size of the coupling effect. Population scatter plots confirmed a significant
432 correlation between the observed coupling effect and the diameter of the moved whisker (Figure
433 3E, Spearman's coefficient $\rho = 0.63$, $P = 1.27 \cdot 10^{-6}$), and less with the diameter of the imaged
434 whisker (Figure 3F, Spearman's coefficient $\rho = 0.14$, $P = 0.034$). We conclude from these data
435 that mechanical coupling is dependent on properties local to the deflected whisker, such as its
436 diameter. Nonetheless, we acknowledge that beyond the gradient of diameter of the deflected
437 whisker, other gradients of mechanical properties of the whiskers, follicles or skin may contribute
438 to the observed asymmetries. Because all these gradients are correlated, it is difficult to
439 disentangle their relative contribution. This is best addressed by manipulation of individual
440 features in a biomechanical model, as we report in a later Results section.

441

442 ***Constraining the whisker tip induces curvature changes***

443 In all these observations, the imaged whisker was unrestrained while other whiskers were
444 deflected. The induced movement consisted in a rotation around the follicle entry with no
445 detectable change in curvature or displacement of the follicle entry point (Figures 1 and 2B). In
446 previous studies modelling the whisker as a rigid anchored beam, changes in curvature have been
447 shown to be proportional to the moment of rotational forces along the whisker (Solomon and

448 Hartmann, 2006; Quist and Hartmann, 2012). Our results above are consistent with the fact that
449 since the whisker shaft was not touching any external object, there were no forces along it, and
450 thus no curvature changes. Mechanical conditions are different when the shaft of the whisker is
451 maintained in a given position or manipulated by a stimulator. The whisker is then constrained
452 both at the follicle level and by the external contact. Forces are generated along the whisker shaft,
453 and the whisker bends. In those conditions, the curvature changes give an estimate of the forces
454 generated along the whisker shaft down to the follicle entry, where mechanoreceptors are
455 located.

456 To investigate these forces during mechanical coupling, we repeated the measures of whisker
457 deformation after introducing the imaged whisker into the standard plastic cylinder attached to
458 our multi-whisker stimulator, in the rest position. In this "Constrained" configuration, deflecting a
459 whisker could still induce a measurable movement in a neighboring whisker (Figure 4A). As
460 expected, the amplitude of the deformation and the change in angle were smaller than in the
461 "Free" condition (note the different horizontal scales for the profiles of Figure 4A). However, we
462 now observed a change in the whisker curvature. These results were confirmed in our population
463 dataset of videography recordings in which one whisker was imaged while its immediate neighbor
464 in the same row was deflected, either "Free" or "Constrained" (Figure 4B and C, $n = 46$).
465 Specifically, changes in angle that were observed in the "Free" condition were correlated with
466 changes in angle of smaller amplitude in the "Constrained" condition (Figure 4B, Spearman's
467 coefficient $\rho = -0.56$, $P = 5.4 \cdot 10^{-5}$), as in the example of Panel A. Additionally, in the
468 "Constrained" condition, changes in curvature were significantly correlated with changes in angle
469 (Figure 4C, Spearman's coefficient $\rho = 0.47$, $P = 0.001$).

470 These results emphasize that in the "Constrained" condition, because of the added external force
471 at the tip counteracting the natural movement of the whisker, rotational forces are generated

472 along the imaged whisker down to its base. As a consequence, below follicle entry, the distribution
473 of forces at the whisker-follicle contact surface is likely to be different in the “Constrained” vs.
474 “Free” condition, leading to possible differences of mechanoreceptor activation.

475

476 ***Deflection of adjacent whiskers at high amplitude evoke action potentials in trigeminal ganglion***
477 ***neurons***

478 The whisker imaging experiments demonstrated that neighboring whiskers and their follicles are
479 indeed distorted when a single whisker is deflected. Next, we wanted to assess whether
480 mechanical coupling could directly elicit spiking activity in primary afferent axons. We recorded
481 extracellularly from trigeminal ganglion neurons while stimulating the ipsilateral whiskers in six
482 anesthetized rats. All 24 whiskers were constrained in their respective stimulators throughout the
483 experiment in order to minimize manipulation of the animal snout during the electrophysiological
484 recordings. Since TG neurons each have a different threshold for evoked activity, we routinely
485 tested several speeds and amplitudes of stimulation to determine both the whisker follicle
486 innervated by each neuron and the stimulation threshold. In each case, we determined a relatively
487 low level of stimulation at which we observed evoked spikes for the deflection of only one whisker
488 out of 24. This is in line with previous studies of TG receptive fields, reported to be monovibrissal
489 (Zucker and Welker, 1969; Gibson and Welker, 1983). For example, the first neuron displayed in
490 Figure 5A responded only to the deflection of whisker E1, and only in the caudal direction (top row
491 of rasters and histograms). There was no spiking for the rostral direction of movement, or for
492 either direction when the stimulation was applied on any of the other 23 whiskers (shown as an
493 example for whisker Delta). We conclude that E1 is the principal whisker (PW) of this neuron.
494 To estimate the impact of mechanical coupling on the firing of this neuron, we then stimulated all
495 whiskers individually at a higher speed (1330°/s vs. 800°/s previously). Spikes were now reliably

496 evoked following the deflection of the adjacent whisker (AW) Delta in the rostral direction (Figure
497 5A, second row of rasters and histograms). This additional response indicates sufficient
498 mechanical coupling between follicles Delta and E1 to induce spikes in the E1-innervating neuron
499 when deflecting Delta. The response disappeared entirely if we removed the E1 whisker from its
500 stimulator, indicating that the “Constrained” state of the PW contributed to the mechanical
501 coupling effect. Interestingly, the direction of movement that had to be applied to the adjacent
502 whisker to evoke spikes was opposite to the preferred direction for the principal whisker.

503 We report here 14 cases of mechanical coupling leading to evoked spikes in TG neurons, out of 14
504 TG recordings for which we were able to test responses to caudal and rostral neighboring whiskers
505 at high deflection speeds (up to 4,000°/s, see Methods). On the summary map of Figure 5B, each
506 arrow indicates coupling from an adjacent whisker, whose deflection evoked spikes in a TG neuron
507 innervating a neighboring follicle. The functional response resulting from mechanical coupling was
508 almost always observed for the stimulation of an immediately adjacent whisker in the same row,
509 although it was always tested for all other 23 whiskers. We observed only one case of coupling
510 across two different rows, from whisker A1 to whisker B2. Interestingly, most coupling effects
511 (10/14, filled arrows) originated from the caudal adjacent whisker, in agreement with the larger
512 mechanical coupling revealed in the videography experiments from immediately caudal whiskers
513 (Figures 2B and 3A). The Example Neuron 2 of Figure 5A displays one of the 4 rostral interactions
514 that we observed (open arrows in Figure 5B). Here, whisker C2 deflections elicited spikes in a C1-
515 innervating neuron. Finally, preferred directions for the principal and adjacent whiskers were
516 usually opposite, except in two cases, one of which is shown in the bottom row of Figure 5A
517 (Example Neuron 3).

518

519 ***Adjacent whisker deflections can modify responses of TG neurons to principal whisker***

520 ***deflections***

521 These recordings confirmed that deflecting an adjacent whisker could induce spiking activity in a
522 TG neuron. However, it should be emphasized that this usually required strong stimulation pulses,
523 from 330 to $\sim 4,000^\circ/\text{s}$, thus above the stimulation thresholds observed for principal whisker
524 stimulation in our sample (usually $100^\circ/\text{s}$ or less). Nonetheless, we reasoned that even
525 subthreshold stimulation of an adjacent whisker could induce deformation of a follicle and
526 modulate the firing properties of mechanoreceptors. We present one example cell suggesting that
527 this subthreshold modulation can indeed occur. The middle row of Figure 6A displays the action
528 potentials and average activity in time of a TG neuron for 36 rostral deflections of its principal
529 whisker D1, for two different speeds (left, $12.5^\circ/\text{s}$, right, $20^\circ/\text{s}$). During the same protocol, we also
530 tested responses obtained when adding a deflection of whisker D2, either in the caudal (top row)
531 or in the rostral (bottom row) direction. In these randomly interleaved trials, D2 was deflected at a
532 subthreshold stimulation level. We observed that the joint stimulation of D2 and D1 led to either
533 more activity (top row, D2 caudally deflected) or less activity (bottom row, D2 rostrally deflected)
534 than the single stimulation of D1. These effects were present for a range of stimulation speeds of
535 the principal whisker, and disappeared at very small speeds, when the PW response itself occurred
536 at a very long latency (Figure 6B). Although we could not test this modulatory effect
537 systematically, it suggests that neighboring whiskers have an ongoing influence on responses to
538 the principal whisker through mechanical coupling.

539

540 ***Mechanical model of two neighboring whiskers and follicles***

541 Videography and electrophysiology experiments give us important but indirect clues about the
542 mechanical interactions between follicles inside the skin. To estimate the transfer of mechanical
543 forces from one follicle to a neighboring one, and gain better understanding of its functional

544 implications, we built a finite-element model of two whiskers and their follicles, linked by a layer
545 of skin which takes into account superficial muscles (Figure 7A). We used geometrical and
546 mechanical parameter values in the ranges reported in the literature (see Methods). The static
547 deformations and forces resulting from the deflection of one whisker were calculated using
548 Solidworks Simulation. The model reproduced the expected induced movement of an adjacent
549 whisker when one whisker is deflected at the tip (Figure 7B; Left: deflected whisker, Middle:
550 adjacent whisker). The change in angle, when the whisker was free in air, reached 0.2° (20% of the
551 imposed deflection), in the same range as the experimental measurement shown in Figure 1, and
552 the external whisker shaft was straight (no curvature). When the whisker was constrained at the
553 tip, it showed changes in curvature along the whisker shaft (Figure 7B, Right), as was observed in
554 the experimental data. The curvature reversed inside the follicle, so that the whisker had an
555 inverted S shape inside the follicle and protruded rostrally. When the whisker was free in air, there
556 was only a C shape bend inside the follicle.

557 We were particularly interested in the forces generated inside the follicles, which are the source of
558 the input signals for downstream neural sensory processing. We extracted the contact pressure of
559 the deflected and adjacent whiskers on their follicles, thus obtaining 2D profiles of forces
560 represented on two cylinders (Figure 7C). For the whisker that was deflected at its tip in a rostral
561 direction, these forces were distributed in several areas: mainly a rostral zone in the very top part
562 and a large caudal zone in the upper middle (Figure 7C). This distribution of forces matches the
563 deformation of the whisker towards the front, i.e. the negative curvature in Figure 7B, Left.

564 Functionally, the upper middle zone of the follicle is thought to contain the highest density of
565 mechanoreceptors (Ebara et al., 2017). Our simulation results suggest that they would be
566 activated because of the deflected whisker bending inside the follicle and pushing internally on
567 that zone.

568 For the neighboring whisker, we further extracted the 1D profiles on the caudal and rostral lines
569 along the cylinder modeling its follicle (Figure 7D). The distribution of contact forces depended on
570 whether the whisker shaft was let free in air or constrained at the tip. Specifically, when it was in
571 the “Constrained” condition, we obtained contact pressure areas mirroring those of the deflected
572 whisker in the upper part of the follicle, with a reduced amplitude (Figure 7C-D). Thus, forces were
573 present in a caudal zone at the top and a rostral zone in the upper middle part of the follicle. This
574 distribution matches the S-shape whisker bending revealed by the displacement and curvature
575 profiles (Figure 7B).

576 By contrast, when the non-manipulated whisker was let free in air, the middle rostral zone of
577 positive contact pressure largely disappeared (Figure 7D, red dashed lines compared to red full
578 lines). This corresponds to the whisker bending smoothly towards the front (Figure 7B). The top
579 caudal zone was still present but contact forces were smaller. Overall, this result confirms that the
580 “Free” and “Constrained” conditions indeed lead to different distributions of forces inside the
581 follicle and thus potentially to different ensembles of activated mechanoreceptors. In the
582 following, we focus on the “Constrained” condition and on contact pressure values in the upper
583 middle zone of the follicle, given its importance in coding whisker deflections.

584 Note that if the imposed deflection is applied in the opposite direction, i.e. caudally, the
585 displacement, curvature and distribution of forces of the deflected and induced whisker-follicle
586 ensembles are essentially symmetrical to the rostral case. The mechanical coupling strength
587 between the two whiskers is thus independent of the direction of stimulation, as in the
588 videography experiments (Figure 2A).

589 Using this simple model, we tested the causal link between whisker diameter and the amplitude of
590 mechanical coupling. We increased or decreased the whisker diameter by about 17% (50 μm),
591 which is in the range of whisker diameter differences between neighbors in a row of the whisker

592 pad. When we modified the diameter of the deflected whisker while keeping the neighboring
593 whisker diameter at 300 μm , the peak contact pressure inside the follicle varied by 40-45% (Figure
594 7E). The curvature along the whisker changed little (350 μm : 7% decrease; 250 μm : 15% increase).
595 However, the whisker stiffness was almost doubled for the 350- μm whisker, and conversely halved
596 for the 250- μm whisker. The bending moment and whisker-follicle forces were thus largely
597 governed by the whisker diameter via the change in stiffness. This result confirms from a
598 biomechanical point of view that the whisker diameter could indeed be a major factor in
599 mechanical coupling effects.

600 We quantified the asymmetry created by these differences in diameter by the peak contact
601 pressure in the upper middle zone (Figure 7F, Left). We found that when the thicker whisker of an
602 asymmetric pair was deflected, it induced a peak contact pressure in the neighboring follicle twice
603 larger than when the thinner whisker was deflected. This ratio is in the range of what has been
604 measured experimentally on induced deflections (Figure 3B, mean change in angle 0.077° vs.
605 0.042° , $n = 14$). Additionally, we observed in the model that the deflection of a whisker of 300- μm
606 diameter had a stronger effect on a 250- μm neighbor than on a 350- μm neighbor (contact
607 pressure 1.26 vs. 0.60 N/cm^2 , Figure 7F, Left, filled square vs. open circle), thus reproducing the
608 asymmetrical results of Figure 3C for a given deflected whisker. We conclude from these
609 simulations that the distribution of mechanical coupling strength observed in the experimnts, as
610 well as the rostro-caudal asymmetry, can be fully explained by the gradient of whisker diameter.

611 Certainly, other elements of the model could be modified in order to study their impact on the
612 mechanical coupling and its anisotropy. Increasing the follicle diameter tended to reduce coupling,
613 probably because of increased mechanical absorption by the follicle. Increasing whisker spacing
614 from 2 to 5 mm had very little effect (6% decrease in peak contact pressure).

615 Given that these geometrical parameters could not explain the mechanical coupling anisotropies,

616 we then sought to test the impact of the different muscles of the whisker pad. Extrinsic muscles in
617 the model were part of the skin volume. We found that modifying the skin thickness had little
618 effect (less than 3% for twice the thickness), even when creating a 2:1 thickness gradient along the
619 rostrocaudal axis. On the other hand, doubling Young's modulus of the skin material increased the
620 peak contact pressure by 60%. Interestingly, it did not change the distribution of the contact
621 forces inside the follicle. Indeed, this distribution is essentially governed by the boundary
622 conditions at both ends of the whisker, and can be changed by modifying those boundaries as in
623 the "Free" vs. "Constrained" conditions (Figure 7B and D). Overall, these results investigating skin
624 parameters suggest that a gradient of skin stiffness might contribute to the caudo-rostral gradient
625 of mechanical coupling observed in the experiments.

626 Finally, we modelled the intrinsic muscle by a stiff oblique rod connecting two rings placed around
627 the follicles (Figure 7F, Right). The presence of this asymmetric element created an asymmetry of
628 coupling between the two whiskers, while decreasing both values. Although the real intrinsic
629 muscle is likely to be weaker than modelled here, this result suggests it could participate to the
630 mechanical coupling asymmetry between whiskers.

631 From this simple model, we conclude that the gradient of mechanical coupling observed in the
632 videography and electrophysiology experiments could be explained largely by the gradient in
633 whisker diameter, with a possible contribution of the intrinsic muscles connecting the follicles.

634 **DISCUSSION**

635 In this study, we show that deflecting a single whisker on the rat snout is accompanied by
636 measurable movements of neighboring whiskers. Moreover, if the deflection is sufficiently strong,
637 it evokes spiking activity in primary afferent neurons innervating the follicles of neighboring
638 whiskers. We use a simple mechanical model to show how transmission of mechanical forces
639 through the skin is responsible for this cross-whisker interaction.

640

641 ***Characteristics of mechanical coupling and possible underlying mechanisms***

642 Both our videography and electrophysiology results emphasized intra-row interactions relative to
643 intra-arc ones (Figures 2B and 5B). This could be due to the particular direction of our stimuli,
644 along the rostrocaudal axis (see below, Methodological considerations). This bias could also arise
645 from the presence of intrinsic muscles between adjacent follicles in a row (Dörfl, 1982; Haidarliu et
646 al., 2010), responsible for pivoting the whisker around the follicle entry during whisking
647 protraction. Recently, several laboratories reported the presence of additional oblique intrinsic
648 muscles further connecting follicles along rows (Grant et al., 2013, 2017; Haidarliu et al., 2017).
649 Together, these intrinsic muscles likely increase the stiffness of the skin particularly along the
650 rostrocaudal direction, thus favoring the transmission of movements and forces along rows
651 compared to arcs. Interestingly, intrinsic muscles can connect a straddler to both anterior follicles
652 (Dörfl, 1982), a pattern corresponding to the interaction of straddlers with both neighbors in our
653 electrophysiological data (Figure 5B).

654 A second striking result concerns the spatial distribution of mechanical coupling across the whisker
655 pad. We found that effects were largely biased to the caudal half of the whisker pad, with an
656 additional ventral emphasis especially in the electrophysiological data (Figures 3D and 5B). These

657 results have led us to hypothesize that the size of the whisker, known to exhibit a strong caudo-
658 ventral bias (Belli et al., 2017), could be an important factor governing the amplitude of
659 mechanical coupling. In fact, many biomechanical studies assume the whisker diameter to be the
660 only parameter distinguishing one whisker from another when describing the preneuronal
661 transformation of contact events into forces at the follicle entry (Boubenec et al., 2012; Quist and
662 Hartmann, 2012; Carvell and Simons, 2017; Oladazimi et al., 2018). Indeed, the hypothesis that
663 mechanical coupling varies due to the gradient of the deflected whisker diameter seems the most
664 parsimonious interpretation of our data. Interestingly, the dependence on the deflected whisker
665 diameter was very strong in the biomechanical simulations, whereas the model was constructed
666 and calibrated without this test in mind. Increasing the diameter of the whisker by about 17%, as
667 is found between neighbors in a row, increases its stiffness by 85%, according to the power law
668 with exponent 4 applying to a cantilevered beam. An identical displacement at the tip thus
669 requires a much larger bending moment, and induces larger contact forces between the whisker
670 and the follicle (Figure 7E). The whisker diameter gradient could thus account for the overall
671 spatial distribution of the cross-whisker coupling effect on the snout.

672 To definitively establish whisker diameter as a main factor in shaping the gradient of mechanical
673 coupling on the whisker pad, several concerns will need to be addressed. First, the expected
674 ventral bias was not clear in our videography data. Unfortunately, we could not test all
675 combinations of deflected and imaged whiskers (see Methodological limitations below).

676 Second, the distribution of coupling effects revealed in the electrophysiology experiments
677 necessarily includes a recording bias. In the trigeminal ganglion, the number of neurons
678 innervating large whisker follicles is higher than for small whiskers (Zucker and Welker, 1969;
679 Welker and Van der Loos, 1986). There could also be a systematic bias in our electrode location in
680 the ganglion, which is known to be loosely topographically organized (Leiser and Moxon, 2006).

681 Nonetheless, the strong caudo-ventral gradient suggests predominant mechanical coupling effects
682 in that part of the pad. Note that we do not rule out that mechanical coupling could potentially
683 influence the firing of any whisker-sensitive TG neuron, provided a neighbor whisker is deflected
684 with sufficiently high magnitude.

685 On top of the spatial gradient, for a given whisker combination, we found an asymmetry favoring
686 mechanical coupling from the caudal to its immediately rostral neighbor, compared to the
687 opposite sequence (Figure 3B). We will consider several possible sources of this asymmetry. First,
688 the systematic gradient in whisker diameter across the pad can suffice to explain a strong
689 asymmetry in coupling inside a given whisker pair, as confirmed by the model simulations (Figure
690 7E-F). This gradient can also explain that deflecting a fixed whisker affects differently its two
691 neighbors (Figure 3C), because the mechanical coupling strength is clearly dependent on the
692 whisker diameter of the neighbor (Figure 7F, Left, filled square vs. open circle). Thus, the rostral vs.
693 caudal asymmetry observed in the experimental data can be fully explained by the gradient in
694 whisker diameter across the pad.

695 Another factor that could play a role in the asymmetry of the mechanical coupling is the intrinsic
696 muscle between follicles. As mentioned already, this muscle is attached to the superficial part of
697 the caudal follicle and skin, and to the deep part of the rostral follicle. We have investigated the
698 potential asymmetrical mechanical effects resulting from this diagonal muscle by adding it to the
699 biomechanical model as a rod connecting the follicles. We found that it could create an
700 asymmetry favoring stronger coupling from the caudal whisker, while at the same time reducing
701 the overall values (Figure 7F, Right). Note that in the simulations, we chose to use the same
702 material for the intrinsic muscle as for the skin and follicles, even though the real muscle is likely
703 to be much less stiff than the tough protective skin layer on the snout. The effect of the intrinsic
704 muscle is thus probably largely overestimated in the model. Overall, we conclude that the intrinsic

705 muscle could contribute to the asymmetry in cross-whisker effects, but that it has probably much
706 less influence than whisker diameter.

707 Other factors beyond whisker diameters and intrinsic muscles could contribute to the amplitude of
708 mechanical coupling and to its asymmetry. For example, the size of follicle elements and
709 surrounding muscles vary in a systematic way, correlated with the average whisker diameter
710 (Haidarliu et al., 2010), and are likely to influence the transmission of forces from one whisker-
711 follicle to another. The superficial extrinsic muscles maxillofacialis and nasolabialis probably stiffen
712 the pad and could thus increase mechanical coupling and its asymmetry, in particular when the
713 muscle tone is high such as in the active exploring state. Moreover, because there are more fibers
714 in the caudal section of the pad, the extrinsic muscles could contribute to the gradient that we
715 observed. The nasolabialis fibers extending from the dorso-caudal region could particularly
716 enhance mechanical coupling in that region compared to the ventro-caudal gradient expected
717 from the gradient in whisker diameter.

718 Our simulations suggested that the size of the follicles and the skin thickness were unlikely to
719 explain the mechanical coupling distribution, but that the stiffness of the skin layer could be
720 important. This opens the possibility that the tone of the extrinsic muscles could have a significant
721 impact. A more detailed model could be built to study specifically the effect of the different
722 whisker pad elements. It could include variations in whisker taper and whisker low-density core
723 (medulla), which have recently been shown to vary across the pad, beyond the expected variations
724 of length and diameter (Belli et al., 2017). Finally, on top of these established gradients, an
725 important source of variability could arise from the current phase of the whisker in the growth
726 cycle, affecting directly its size (Ibrahim and Wright, 1975).

727

728 ***Distribution of forces activating mechanoreceptors***

729 The biomechanical model was constructed in order to qualitatively bridge the gap between
730 external whisker deformations and spiking activity in primary afferent neurons. We included only
731 one element per whisker and follicle, embedded in a skin sheet. Minimal calibration was necessary
732 to produce induced deformations compatible with experimental measures. With this simple
733 model, the whisker shaft, when deflected, compresses the leading edge of the top of the follicle,
734 as well as the trailing edge at a deeper location because of internal bending. This agrees with a
735 recent ex-vivo study (Whiteley et al., 2015) describing a distribution of strain along the depth of
736 the follicle in which compression and dilation zones alternate. When the neighboring whisker is
737 constrained at its tip, induced contact forces on its follicle adopt a mirror configuration with a
738 smaller amplitude (Figure 7C). As a consequence, a mechanoreceptor located in a zone of
739 compression for an imposed deflection of its principal whisker will be best stimulated if the
740 adjacent whisker is deflected in the opposite direction. Indeed, in most (12/14) TG neurons, we
741 observed that the preferred direction of deflection for the adjacent whisker was opposite to the
742 preferred direction for the principal whisker (Figure 5).

743 The density of mechanoreceptors is highest in the top half of the follicle, and more specifically in
744 the ring sinus region (Ebara et al., 2017). In a recent study combining anatomical and functional
745 characterization, the most numerous and most responsive TG neurons were found to be those
746 terminating with club-like endings in the ring sinus region. These terminals are particularly suited
747 to encode a specific direction of movement (Tonomura et al., 2015). This class of
748 mechanoreceptors has previously been underestimated because of their tiny axonal endings,
749 easily mistaken as cut axons. Interestingly, our model does predict contact forces in this region
750 induced by deflection of an adjacent whisker, particularly when the principal whisker is
751 “Constrained” (Figure 7).

752 In this respect, we have systematically explored two different conditions in the experiments and

753 the model: the “Free” and “Constrained” conditions. It is interesting to note that constraining the
754 neighboring whisker led to increased curvature changes along the shaft, and at the same time to
755 increased responses in the putative mechanoreceptors of the associated follicle. This is in line with
756 the idea that the rotational moment at the base of the whisker, known to be proportional to the
757 curvature, is indeed what is encoded by mechanoreceptors, both in the passive and active states
758 (Quist & Hartmann, 2012; Campagner et al., 2016). The model simulations, by illustrating the
759 distribution of forces inside the follicle, offer a mechanistic explanation. When the whisker is
760 “Constrained”, a large contact pressure zone is present in the ring sinus region compared to the
761 “Free” condition (Figure 7C). Thus, the model confirms that the external forces on the whisker
762 produce a bending moment along the shaft which causes pressure forces in a specific localized
763 zone of the follicle. Mechanoreceptors terminating in this zone are activated, encoding directional
764 and amplitude information about the deflection event.

765

766 ***Functional relevance***

767 Our results imply that the skin tissue and muscles making up the whisker pad transmit forces
768 between follicles, and that this additional force field can, depending on its direction, either
769 counteract or augment the ongoing forces due to external events on the whisker shaft. It brings
770 forward a theory that has already been proposed earlier, namely that the whisker system, despite
771 its discreteness, could function as a continuous sensory organ just like the skin (Simons, 1995).

772 From a practical point of view, our results imply that there can be no pure single whisker
773 movement, because the biomechanical forces move all elements of the pad (muscles, follicles,
774 whiskers) in an automatic fashion. These induced deformations could reach up to 10-20% in our
775 experimental conditions. Their impact on sensory processing should be considered. It has been
776 shown that the most sensitive primary afferents respond to extremely small deflections of

777 amplitude less than 0.01° , and one third of all afferents have a velocity threshold below $3^\circ/s$
778 (Gibson and Welker, 1983). For very small single-whisker deflections, only a handful of trigeminal
779 ganglion neurons spike action potentials, and all these neurons are likely to innervate the
780 deflected whisker, conforming to the labelled line hypothesis. When deflection parameters
781 increase, more and more mechanoreceptors are activated, including some with low thresholds
782 located in surrounding follicles. Upstream, we thus expect some amount of divergence of the
783 sensory signal from a single whisker to trigeminal ganglion neurons innervating other whiskers,
784 and further, to surrounding barrelettes. This divergence will of course depend on the particular
785 whisker considered, and we propose that the whisker diameter is an important parameter of the
786 extent of this spatial spread.

787 During stimulation of several whiskers overlapping in time, our results suggest that modulation of
788 responses to the principal whisker by the simultaneous deflection of surrounding whiskers is also
789 already present at the trigeminal ganglion level. The example neuron of Figure 6 shows that even
790 for very low deflection values, mechanical coupling can modify responses to external events
791 occurring on the principal whisker. As confirmed by the model, even low deflections modulate the
792 distribution of forces present in neighboring follicles. When two deflections occur at the same
793 time, forces inside the follicles will be enhanced for opposite directions of movement, or on the
794 contrary attenuated. Functionally, these ongoing mechanical effects could for example emphasize
795 detection of surfaces tending to bring whiskers together, such as corners.

796 In our view, this peripheral cross-whisker interaction can be thought of as a first nonlinearity in the
797 information processing pathway, before the other known nonlinearities at the trigeminal nuclei,
798 thalamic and cortical levels. Several laboratories, including our own, have reported that cortical
799 neurons are able to extract multi-whisker features of tactile scenes (review in Estebanez et al.,
800 2018), suggesting that cortical neuronal tuning could underlie the ability of animals to identify

801 relevant perceptual features. The existence of multi-whisker interactions within the whisker pad
802 do not contradict these findings. Rather, it confirms that multi-whisker integration starts already
803 before the cortex. In other words, we need to be careful about claiming that nonlinearities
804 observed in the cortex are not already present at a subcortical or even peripheral level. Such
805 mechanisms have been known to exist for a long time in the trigeminal nuclei (Minnery and
806 Simons, 2003; Timofeeva et al., 2004), and have been described also in the thalamus, including the
807 extraction of high-order features like global apparent motion (Ego-Stengel et al., 2012). In this last
808 study, multi-whisker selectivity was shown to be present in the thalamus but to a lesser extent
809 than in the cortex, and to be amplified at the cortical level. Our current view on tactile processing
810 mechanisms is that intracortical circuitry builds an additional layer of computation which uses the
811 results of nonlinearities in the previous stages of the system to transform the tactile signals
812 further. Future experiments should help to understand the precise role of each of these stages.

813

814 ***Methodological considerations***

815 Following the description of a single case of cross-whisker spiking response in a TG neuron
816 (Simons, 1985), this is the first study directly investigating mechanical coupling between whiskers
817 and its consequences on neuronal encoding of tactile information. In most laboratories including
818 our own, only relatively low-amplitude low-speed stimuli are routinely implemented. Indeed, a
819 known limitation of piezoelectric stimulators, widely used in the field, is that high velocity stimuli
820 quickly produce ringing (Jacob et al., 2010), thereby constraining their useful range. In the
821 summary drawn by Ritt and collaborators (2008), they concluded that the highest speed explored
822 in electrophysiological studies across laboratories was 2,500°/s, and the highest amplitude of
823 deflection was 3°. Here, we raised the deflection amplitude to 3° or more and the speed up to
824 4,000°/s in order to reveal direct mechanical cross-whisker effects on neurons. These parameters

825 could only be achieved by placing the stimulator close to the whisker base, a procedure performed
826 very carefully under the microscope in order to touch neither the fur nor a neighboring whisker or
827 stimulator.

828 The use of high-resolution videography allowed us to track the profile of whiskers with extreme
829 precision, below 1 μm and at 1 kHz, using minimal image processing. We quantified mechanical
830 coupling effects in a systematic way by measuring the deformation profile of whiskers. We only
831 imaged whiskers for which the shaft was relatively horizontal, thus in focus along its length, and
832 unobstructed by bulging of the pad or by excessive fur. Future experiments could take advantage
833 of new cameras which are more compact and easier to position with different angles around the
834 animal, potentially allowing tracking of all macrovibrissae.

835 The experiments were performed on an anesthetized preparation in order to ensure stable
836 conditions and full control of the stimulus. Assessing the magnitude of cross-whisker coupling in
837 awake behaving animals will be particularly challenging. Animals will have to be trained, for
838 example by head-fixation, in order to enable high-resolution imaging of their whiskers.
839 Importantly, the awake preparation will introduce multiple factors which can influence the state of
840 the follicles and that will require monitoring. The baseline tonus of skin muscles involved in the
841 whisker array positioning is likely to be larger in the awake animal, possibly transmitting
842 mechanical energy more efficiently across follicles. By using anesthesia, we may in fact have
843 underestimated the coupling effect. Electromyographic recordings have further shown that the
844 pad muscles are tightly regulated by a brainstem feedback loop triggered by whisker contact
845 (Nguyen and Kleinfeld, 2005; Bellavance et al., 2017). Accompanying changes in the pressure
846 inside the follicle blood sinus could affect the receptors dynamic range of encoding. The
847 magnitude of cross-whisker coupling is thus likely to vary continuously during the awake state,
848 even in a passive condition.

849 When animals explore their environment, they actively move their whiskers in a coordinated way,
850 including whisking but also asymmetric behaviors (Grant et al, 2009; Sofroniew & Svoboda, 2015).
851 The activation of the pad musculature controls rostrocaudal translation of follicles, along with the
852 protraction of individual whiskers and more subtle deformations (pad bulging, whisker torsion...).

853 In our study, we have purposefully avoided these internally-generated movements and focused on
854 mechanical coupling effects at rest, extracting whisker profile deviations from a stable baseline. In
855 an active animal, evaluating the impact of cross-whisker effects will require an analysis that can
856 disentangle the movements due to active behavior from the movements due to skin coupling. We
857 hypothesize that the passive mechanical coupling effects that we have described add to the
858 underlying global movements of the different structures of the whisker pad. Thus, an external
859 touch on one whisker will modify the trajectory of that whisker but also of neighboring whiskers
860 relative to what it would have been without that touch. How this superposition of internally and
861 externally generated deformations of follicles and whiskers translates into patterns of
862 mechanoreceptor activation will have to be investigated in future studies.

863

864 **REFERENCES**

- 865 Arnold PB, Li CX, Waters RS (2001) Thalamocortical arbors extend beyond single cortical barrels:
866 an in vivo intracellular tracing study in rat. *Exp Brain Res* 136:152-168.
- 867 Axelrad H, Verley R, Farkas E (1976) Responses evoked in mouse and rat SI cortex by vibrissa
868 stimulation. *Neurosci Lett* 3:265-274.
- 869 Bagdasarian K, Szwed M, Knutsen PM, Deutsch D, Derdikman D, Pietr M, Simony E, Ahissar E
870 (2013) Pre-neuronal morphological processing of object location by individual whiskers. *Nat*
871 *Neurosci* 16:622-631.
- 872 Bellavance MA, Takatoh J, Lu J, Demers M, Kleinfeld D, Wang F, Deschênes M (2017) Parallel
873 inhibitory and excitatory trigemino-facial feedback circuitry for reflexive vibrissa
874 movement. *Neuron* 95:673-682.
- 875 Belli HM, Yang AET, Bresee CS, Hartmann MJZ (2017) Variations in vibrissal geometry across the
876 rat mystacial pad: base diameter, medulla, and taper. *J Neurophysiol* 117:1807-1820.
- 877 Bernardo KL, McCasland JS, Woolsey TA (1990) Local axonal trajectories in mouse barrel cortex.
878 *Exp Brain Res* 82:247-53.
- 879 Boubenec Y, Claverie LN, Shulz DE, Debrégeas G (2014) An amplitude modulation/demodulation
880 scheme for whisker-based texture perception. *J Neurosci* 34:10832-10843.
- 881 Boubenec Y, Shulz DE, Debrégeas G (2012) Whisker encoding of mechanical events during active
882 tactile exploration. *Front Behav Neurosci* 6:74.
- 883 Campagner D, Evans MH, Bale MR, Erskine A, Petersen RS (2016) Prediction of primary
884 somatosensory neuron activity during active tactile exploration. *eLife* 5:e10696.
- 885 Carl K, Hild W, Mämpel J, Schilling C, Uhlig R, Witte H (2012) Characterization of statical properties
886 of rat's whisker system. *IEEE Sensors J* 12:340-349.

887 Carvell GE, Simons DJ (1995) Task- and subject-related differences in sensorimotor behavior during
888 active touch. *Somatosens Mot. Res* 12:1-9.

889 Carvell GE, Simons DJ (2017) Effect of whisker geometry on contact force produced by vibrissae
890 moving at different velocities. *J Neurophysiol* 118:1637-1649.

891 Deschênes M, Urbain N (2009) Vibrissal afferents from trigeminus to cortices. *Scholarpedia*
892 4:7454.

893 Dörfl J (1982) The musculature of the mystacial vibrissae of the white mouse. *J Anat* 135:147-54.

894 Dykes RW (1975) Afferent fibers from mystacial vibrissae of cats and seals. *J Neurophysiol* 38:650-
895 62.

896 Ebara S, Furuta T, Kumamoto K (2017) Vibrissal mechanoreceptors. *Scholarpedia* 12:32372.

897 Ebara S, Kumamoto K, Matsuura T, Mazurkiewicz JE, Rice FL (2002) Similarities and differences in
898 the innervation of mystacial vibrissal follicle-sinus complexes in the rat and cat: a confocal
899 microscopic study. *J Comp Neurol* 449:103-119.

900 Ego-Stengel V, Le Cam J, Shulz, DE (2012) Coding of apparent motion in the thalamic nucleus of the
901 rat vibrissal somatosensory system. *J Neurosci* 32:3339-3351.

902 Estebanez L, Férézou I, Ego-Stengel V, Shulz DE (2018) Representation of tactile scenes in the
903 rodent barrel cortex. *Neuroscience* 368:81-94.

904 Gibson JM, Welker WI (1983) Quantitative studies of stimulus coding in first-order vibrissa
905 afferents of rats. 1. Receptive field properties and threshold distributions. *Somatosens Res*
906 1:51-67.

907 Gottschaldt KM, Iggo A, Young DW (1973) Functional characteristics of mechanoreceptors in sinus
908 hair follicles of the cat. *J Physiol* 235.2:287-315.

909 Grant RA, Mitchinson B, Fox CW, Prescott TJ (2009) Active touch sensing in the rat: anticipatory
910 and regulatory control of whisker movements during surface exploration. *J Neurophysiol*

911 101:862-874.

912 Grant RA, Delaunay MG, Haidarliu S (2017) Mystacial Whisker Layout and Musculature in the
913 Guinea Pig (*Cavia porcellus*): A Social, Diurnal Mammal. *Anat Rec* 300:527-536.

914 Grant RA, Haidarliu S, Kennerley NJ, Prescott TJ (2013) The evolution of active vibrissal sensing in
915 mammals: evidence from vibrissal musculature and function in the marsupial opossum
916 *Monodelphis domestica*. *J Exp Biol* 216:3483-3494.

917 Haidarliu S (1996) An anatomically adapted, injury-free headholder for guinea pigs. *Physiol Behav*
918 60:111-4.

919 Haidarliu S, Simony E, Golomb D, Ahissar E (2010) Muscle architecture in the mystacial pad of the
920 rat. *Anat Rec* 293:1192-1206.

921 Haidarliu S, Bagdasarian K, Shinde N, Ahissar E (2017) Muscular Basis of Whisker Torsion in Mice
922 and Rats. *Anat Rec* 300:1643-1653.

923 Hartmann MJ, Johnson NJ, Towal RB, Assad C (2003) Mechanical characteristics of rat vibrissae:
924 resonant frequencies and damping in isolated whiskers and in the awake behaving animal. *J*
925 *Neurosci* 23:6510-6519.

926 Hobbs JA, Towal RB, Hartmann MJZ (2016) Spatiotemporal Patterns of Contact Across the Rat
927 Vibrissal Array During Exploratory Behavior. *Front Behav Neurosci* 9:356.

928 Ibrahim L, Wright EA (1975) The growth of rats and mice vibrissae under normal and some
929 abnormal conditions. *J Embryol Exp Morphol* 33:831-844.

930 Jacob V, Estebanez L, Le Cam J, Tiercelin J-Y, Parra P, Parésys G, Shulz DE (2010) The Matrix: a new
931 tool for probing the whisker-to-barrel system with natural stimuli. *J Neurosci Methods*
932 189:65-74.

933 Jacquin MF, Chiaia NL, Haring JH, Rhoades RW (1990) Intersubnuclear connections within the rat
934 trigeminal brainstem complex. *Somatosens Mot Res* 7:399-420.

935 Kim JN, Koh KS, Lee E, Park SC, Song WC (2011) The morphology of the rat vibrissal follicle-sinus
936 complex revealed by three-dimensional computer-aided reconstruction. *Cells Tissues*
937 *Organs* 193:207-214.

938 Knutsen PM, Pietr M, Ahissar E (2006) Haptic object localization in the vibrissal system: behavior
939 and performance. *J Neurosci* 26:8451-64.

940 Krupa DJ, Matell MS, Brisben AJ, Oliveira LM, Nicolelis MA (2001) Behavioral properties of the
941 trigeminal somatosensory system in rats performing whisker-dependent tactile
942 discriminations. *J Neurosci* 21:5752-63.

943 Lavallée P, Deschênes M (2004) Dendroarchitecture and lateral inhibition in thalamic barreloids. *J*
944 *Neurosci* 24:6098-6105.

945 Leiser SC, Moxon KA (2006) Relationship between physiological response type (RA and SA) and
946 vibrissal receptive field of neurons within the rat trigeminal ganglion. *J Neurophysiol*
947 95:3129-3145.

948 Ma PM, Woolsey TA (1984) Cytoarchitectonic correlates of the vibrissae in the medullary
949 trigeminal complex of the mouse. *Brain Res* 306:374-9.

950 Minnery BS, Simons DJ (2003) Response properties of whisker-associated trigeminothalamic
951 neurons in rat nucleus principalis. *J Neurophysiol* 89:40-56.

952 Narayanan RT, Egger R, Johnson AS, Mansvelder HD, Sakmann B, de Kock CPJ, Oberlaender M
953 (2015) Beyond Columnar Organization: Cell Type- and Target Layer-Specific Principles of
954 Horizontal Axon Projection Patterns in Rat Vibrissal Cortex. *Cereb Cortex* 25:4450-4468.

955 Neimark MA, Andermann ML, Hopfield JJ, Moore CI (2003) Vibrissa resonance as a transduction
956 mechanism for tactile encoding. *J. Neurosci* 23:6499-6509.

957 Nguyen QT, Kleinfeld D (2005) Positive feedback in a brainstem tactile sensorimotor loop. *Neuron*
958 45:447-457.

959 Oladazimi M, Brendel W, Schwarz C (2018) Biomechanical Texture Coding in Rat Whiskers. *Sci Rep*
960 8:11139.

961 Quist BW, Hartmann MJZ (2012) Mechanical signals at the base of a rat vibrissa: the effect of
962 intrinsic vibrissa curvature and implications for tactile exploration. *J Neurophysiol*
963 107:2298-2312.

964 Schneider JS, Denaro FJ, Olazabal UE, Leard HO (1981) Stereotaxic atlas of the trigeminal ganglion
965 in rat, cat, and monkey. *Brain Res Bull* 7:93-95.

966 Sherman D, Oram T, Harel D, Ahissar E (2017) Attention Robustly Gates a Closed-Loop Touch
967 Reflex. *Curr Biol* 27:1836-1843.e7.

968 Simons DJ (1978) Response properties of vibrissa units in rat SI somatosensory neocortex. *J*
969 *Neurophysiol* 41:798-820.

970 Simons DJ (1985) Temporal and spatial integration in the rat SI vibrissa cortex. *J Neurophysiol*
971 54:615-35.

972 Simons DJ (1995) Neuronal integration in the somatosensory whisker/barrel cortex. *Cerebral*
973 *Cortex*, vol. 11, *The Barrel Cortex of Rodents* (Jones EG & Diamond IT, Eds) 11:263-297.

974 Sofroniew NJ, Svoboda K (2015) Whisking. *Curr. Biol.* 25:R137-R140.

975 Solomon JH, Hartmann MJ (2006) Biomechanics: robotic whiskers used to sense features. *Nature*
976 443:525.

977 Timofeeva E, Lavallée P, Arsenault D, Deschênes M (2004) Synthesis of multiwhisker-receptive
978 fields in subcortical stations of the vibrissa system. *J Neurophysiol* 91:1510-5.

979 Tonomura S, Ebara S, Bagdasarian K, Uta D, Ahissar E, Meir I, Lampl I, Kuroda D, Furuta T, Furue H,
980 Kumamoto K (2015) Structure-function correlations of rat trigeminal primary neurons:
981 Emphasis on club-like endings, a vibrissal mechanoreceptor. *Proc Jpn Acad Ser B Phys Biol*
982 *Sci* 91:560-576.

- 983 Van der Loos H (1976) Barreloids in mouse somatosensory thalamus. *Neurosci Lett* 2:1-6.
- 984 Vincent S (1913) The tactile hair of the white rat. *J. Comp Neurol* 23:1-36.
- 985 Voges D, Carl K, Klauer GJ, Uhlig R, Schilling C, Behn C, Witte H (2012) Structural characterization of
986 the whisker system of the rat. *IEEE Sensors J* 12:332-339.
- 987 Voisin DL, Doméjean-Orliaguet S, Chalus M, Dallel R, Woda A (2002) Ascending connections from
988 the caudal part to the oral part of the spinal trigeminal nucleus in the rat. *Neuroscience*
989 109:183-193.
- 990 Welker E, Van der Loos H (1986) Quantitative correlation between barrel-field size and the sensory
991 innervation of the whiskerpad: a comparative study in six strains of mice bred for different
992 patterns of mystacial vibrissae. *J Neurosci* 6:3355-73.
- 993 Whiteley SJ, Knutsen PM, Matthews DW, Kleinfeld D (2015) Deflection of a vibrissa leads to a
994 gradient of strain across mechanoreceptors in a mystacial follicle. *J Neurophysiol* 114:138-
995 145.
- 996 Woolsey TA, Van der Loos H (1970) The structural organization of layer IV in the somatosensory
997 region (SI) of mouse cerebral cortex. The description of a cortical field composed of discrete
998 cytoarchitectonic units. *Brain Res* 17:205-42.
- 999 Zucker E, Welker WI (1969) Coding of somatic sensory input by vibrissae neurons in the rat's
1000 trigeminal ganglion. *Brain Res* 12:138-56.

1001 **FIGURE LEGENDS**

1002

1003 **Figure 1. An imposed 1° deflection of whisker C1 induces a rotation of whisker C2 around its**
1004 **follicle entry.**

1005 A, Raw image of the region of interest captured while studying the effect upon whisker C2 of a
1006 ramp-plateau-ramp deflection of whisker C1. The time course of the C1 deflection is indicated
1007 below the image, along with the color code for twenty successive frames acquired at 1 kHz during
1008 the up-ramp and plateau of the pulse. The C1 and C2 whisker profiles calculated from these
1009 twenty frames are superimposed on the image. B, The same twenty raw profiles are displayed
1010 after applying a magnification factor (dilation) of gain 20 in the direction orthogonal to the
1011 whisker. This anisotropic manipulation, solely used for display, was necessary in order to
1012 effectively observe the induced displacements. With these scales, the whisker profiles appear
1013 bumpy as a consequence of irregularities of the shaft and camera pixelization. Grey lines, second-
1014 order polynomial fits, extrapolated down to follicle entry estimates. C, Deformation calculated by
1015 subtracting the profile right before the start of the deflection, and after smoothing with a time
1016 window of 5 (C1) or 10 (C2) points solely for visual display. Note that the horizontal scales are
1017 different for the two whiskers. Curvature changes could be reliably visualized on these plots,
1018 whereas they were difficult to see before the subtraction. D, Time course of displacement, change
1019 in angle and change in curvature for the two whiskers at three different levels along the shaft (Tip,
1020 Middle, Follicle). In this Figure and others, “Tip” indicates the point at which the stimulation
1021 contacts the whisker shaft. The induced deflection on C2 is a rigid rotation around the follicle
1022 entry, with no curvature change.

1023

1024 **Figure 2. Spatial map of mechanical coupling effects on whisker C2 from other whiskers on the**
1025 **pad.**

1026 A, Time course of the whisker angle at the follicle level while deflecting every other whisker on the
1027 pad either in a caudal (left) or rostral (right) direction. Traces were aligned around their mean
1028 calculated in the 10ms window before the stimulus. Strad., Straddlers arc; A-E indicate rows. B,
1029 Displacement, Change in angle, and Change in curvature at the follicle level quantified in the time
1030 window 10 to 20 ms after stimulation (plateau of the pulse), and pooled over rostral and caudal
1031 directions (median values over 7 rats).

1032

1033 **Figure 3. Mechanical coupling between neighbors follows a systematic gradient on the whisker**
1034 **pad.**

1035 A, Median change in angle for a given imaged whisker when its caudal neighbor (filled circles) or
1036 rostral neighbor (open circles) was moved (n = 26). The change in angle was significantly higher
1037 when the caudal whisker was moved (Wilcoxon signed-rank test, $P = 1.2 \cdot 10^{-5}$). In this and following
1038 panels, filled (resp. open) arrows indicate mechanical coupling due to deflection of a caudal (resp.
1039 rostral) whisker. B, Median change in angle for a given whisker combination when the caudal
1040 whisker was moved and the rostral whisker was imaged (filled circles), vs. when the rostral
1041 whisker was moved and the caudal whisker was imaged (open circles) (n = 14). The change in
1042 angle was significantly higher when the caudal whisker was moved (Wilcoxon signed-rank test, $P =$
1043 0.0023). C, Median change in angle for a given deflected whisker when its caudal neighbor (open
1044 circles) or rostral neighbor (filled circles) was imaged (n = 5). The change in angle was significantly
1045 higher when the rostral whisker was imaged (Wilcoxon signed-rank test, $P = 0.043$). D, Summary of
1046 the mechanical coupling effect pooled across experiments. The width of each arrow indicates the
1047 mean change in angle induced on one whisker (located at the end of the arrow) while a

1048 neighboring whisker (located at the start of the arrow) was deflected (n = 52 effects tested on 6
1049 rats; 1 to 3 data points per arrow, except 6 data points for C2 imaged). Circles indicate the median
1050 diameter of each whisker (n = 4 rats). E, Median change in angle as a function of the diameter of
1051 the whisker moved (n = 48). There was a significant positive correlation between these variables
1052 (Spearman's coefficient $\rho = 0.63$, $P = 1.3 \cdot 10^{-6}$). F, Median change in angle as a function of the
1053 diameter of the whisker imaged (n = 48). These variables were not significantly correlated
1054 (Spearman's coefficient $\rho = 0.14$, $P = 0.034$).

1055

1056 **Figure 4. Constraining the whisker tip results in a curvature change.**

1057 A, Top, Deformation profiles and fits for a whisker either free (left) or constrained at its tip (right)
1058 while its neighbor is being deflected. Conventions as in Figure 1. A 10-point smoothing procedure
1059 was applied solely for visual display. Note that the horizontal scales are different in the two
1060 conditions. Bottom, Time course of the change in angle and change in curvature at three different
1061 levels along the shaft (Tip, Middle, Follicle) for the two conditions. The induced movement was a
1062 rigid rotation in the "Free" condition, and a bend of the whisker in the "Constrained" condition. B,
1063 Change in angle near the tip of the whisker in the "Constrained" condition vs. in the "Free"
1064 condition (n = 46; Spearman's coefficient $\rho = -0.56$, $P = 5.4 \cdot 10^{-5}$). For this graph and the next,
1065 each point represents one combination of whiskers. We calculated the median value over the 8
1066 trials (4 rostral and 4 caudal, mirrored), and the error bars indicate the 25th and 75th percentiles. C,
1067 Change in curvature in the "Constrained" condition vs. change in angle in the "Free" condition (n =
1068 46; Spearman's coefficient $\rho = 0.47$, $P = 0.001$). The very large error bar for one point comes
1069 from one case of different absolute values between rostral and caudal evoked movements.

1070

1071 **Figure 5. Primary afferent neurons fire in response to their principal whisker and to a coupled**

1072 **neighbor whisker.**

1073 A, Action potential raster plots and peri-stimulus time histograms (PSTHs, 1ms bins) of the spiking
1074 activity of three example neurons, evoked by stimulation of their principal whisker (PW) and an
1075 adjacent whisker (AW) for which mechanical coupling was revealed. Plots in the left (resp. right)
1076 two columns display responses to deflections of the adjacent (resp. principal) whisker, whether it
1077 is the rostral or caudal whisker of the pair, for caudal and rostral deflections as depicted above the
1078 columns. The stimulation time course is shown below each histogram. For Example Neuron 1,
1079 spiking activity is shown for two different stimulation levels. For each neuron, the response to the
1080 PW in the PW preferred direction is indicated with a white background. The response to the AW in
1081 the AW preferred direction is indicated with a gray background, highlighting the mechanical
1082 coupling effect at high stimulation levels. Neuron 1, low stim. parameters: 4° , $800^\circ/\text{s}$, $n = 53$ trials;
1083 high stim. parameters: 4° , $1330^\circ/\text{s}$, $n = 42$ trials; Neuron 2: 3° , $300^\circ/\text{s}$, $n = 60$ trials; Neuron 3, PW
1084 (D1) parameters: 4° , $1330^\circ/\text{s}$, AW (Delta) parameters: $\sim 11^\circ$, $\sim 3800^\circ/\text{s}$; $n = 68$ trials. In this last case,
1085 the piezo tip for Delta was advanced to about 3 mm from follicle entry. B, Summary of mechanical
1086 coupling effects resulting in spiking activity. Each arrow indicates that spiking activity could be
1087 elicited in a neuron with its PW located at the end of the arrow, while a neighboring AW, located
1088 at the start of the arrow, was deflected ($n = 14$ neurons on 6 rats). Filled (resp. open) arrows
1089 indicate cases where the AW was a caudal (resp. rostral) neighbor. Darker whisker symbols
1090 indicate whiskers for which we obtained at least one primary afferent recording on which we were
1091 able to thoroughly test responses.

1092

1093 **Figure 6. Mechanical coupling between whiskers can modulate the response of a primary**
1094 **afferent neuron to its principal whisker.**

1095 A, Raster plots and PSTHs of response of a neuron to rostral deflections of its PW at two different

1096 speed levels (left, 12.5°/s; right, 20°/s), while its AW is either deflected caudally (top row), not
1097 deflected (middle row), or deflected rostrally (bottom row). B, Evoked response (mean +/- SEM in
1098 the time window from the start of stimulation to 10ms after the end of the PW ramp) for 8 speed
1099 levels, n = 36 trials each. Asterisks indicate a significant effect of the AW direction (Welch's
1100 unpaired t-test, $P \leq 0.01$).

1101

1102 **Figure 7. A simple finite-element model predicts the location of mechanoreceptor activation due**
1103 **to mechanical coupling and the impact of whisker diameter.**

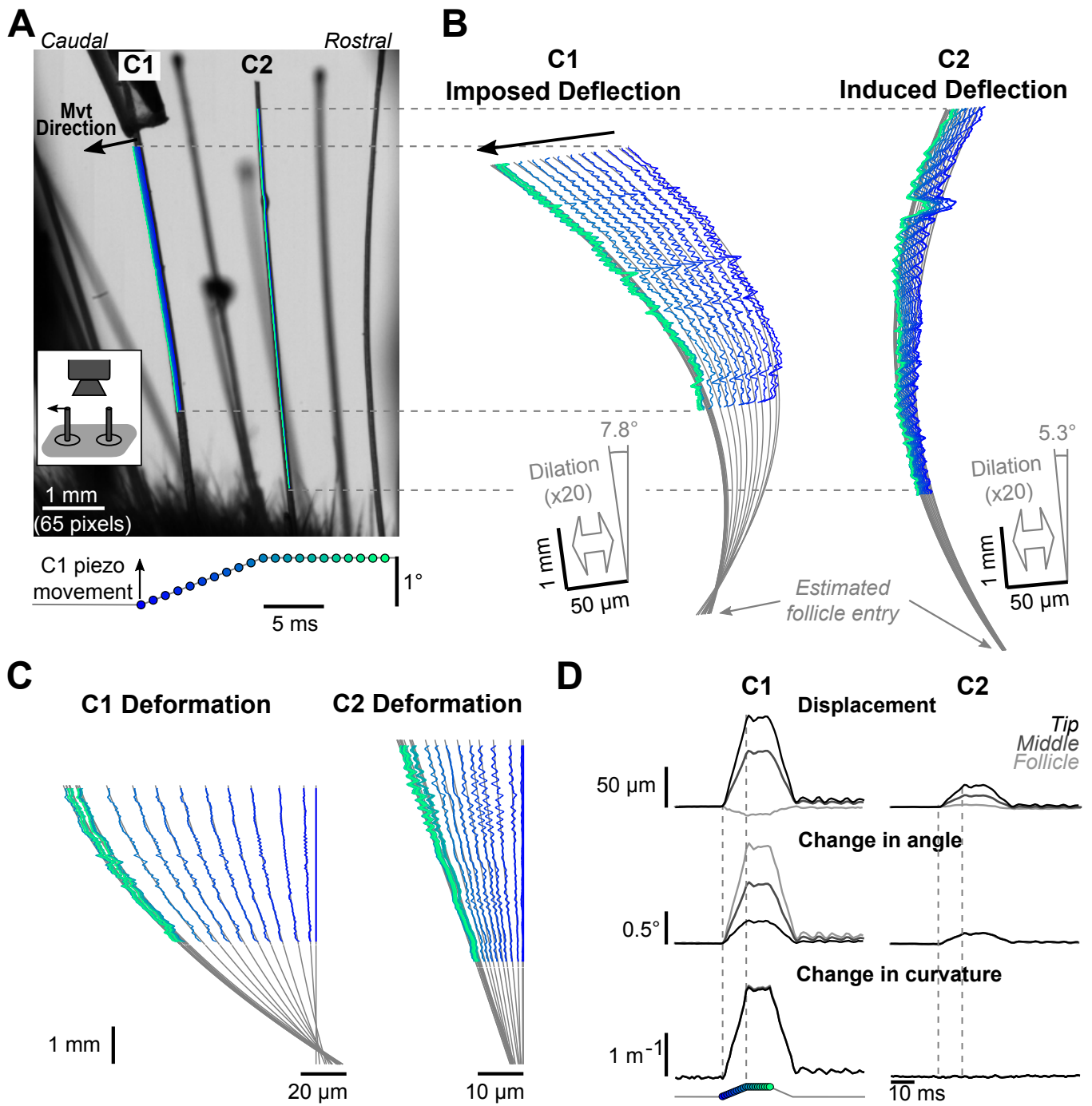
1104 A, Schematics of the model. Whiskers are represented as slender cylinders inside the follicles. The
1105 base of the whiskers and cylinders is fixed. The skin is modelled by a sheet embedding the top of
1106 the follicles. On this schematic, the front right quarter of the model has been removed to show the
1107 whisker-follicle arrangement. The left whisker is deflected by moving its tip, while the right
1108 whisker is either left free or constrained. Caudal is arbitrarily set to the left. Note that some
1109 dimensions have been altered to better show the overall structure. B, Displacement and Curvature
1110 along the two whiskers. The profiles are shown for 10 deflections of 0.1 to 1°, thus corresponding
1111 to experimental profiles of Figures 1 and 4. Negative curvature corresponds to a C bend and
1112 positive curvature to its mirror image. C, snapshot from SolidWorks Simulation of the contact
1113 pressure at the whisker-follicle interface, for the deflected whisker on the left and the neighbor
1114 whisker on the right. The color scale was adjusted to best show the distribution of pressure; the
1115 overall maximum value was 30 N/cm². D, Contact pressure on the caudal and rostral edges of the
1116 whisker-follicle interface for the induced deflection. Solid lines are for the "Constrained"
1117 condition, dashed lines for the "Free" condition. A 2-point running average was performed to
1118 attenuate mesh size artifacts. E, Same curves as in D for the induced deflection in the
1119 "Constrained" case, but varying the diameter of the deflected whisker from 250 μm to 350 μm.

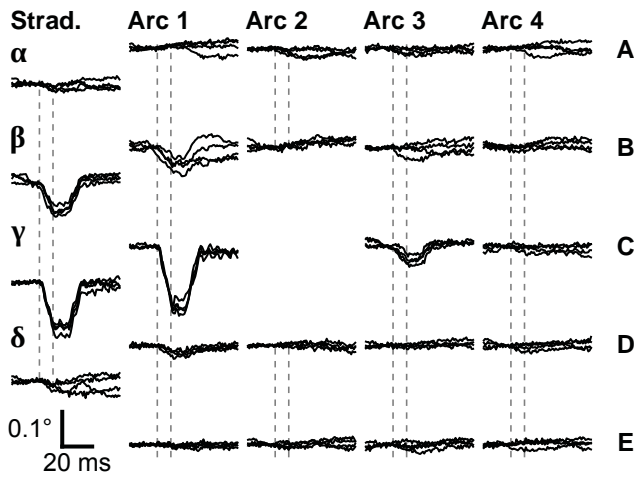
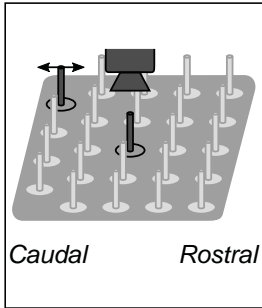
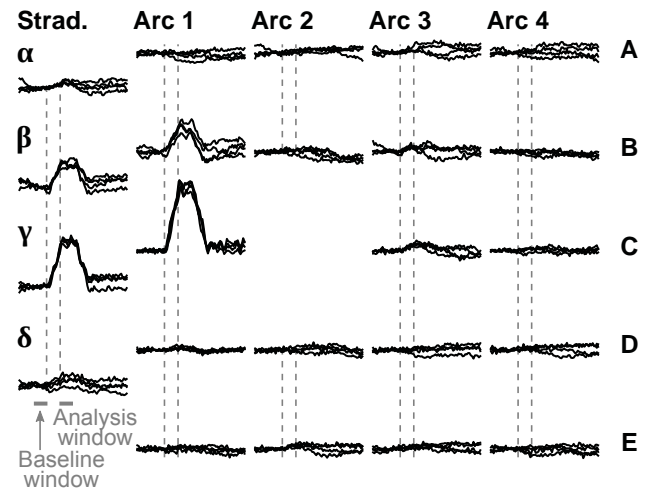
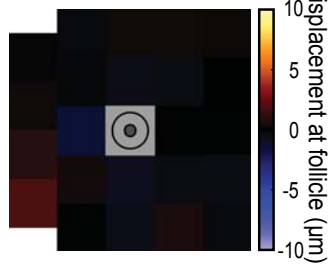
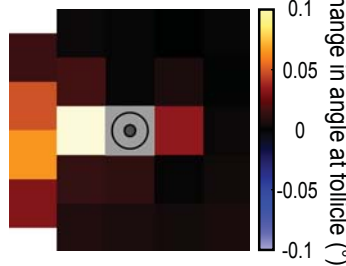
1120 Note that the contact pressure scale is different than in D. F, Left, Peak induced contact pressure
1121 in the upper middle zone for three different combinations of whisker diameters. The thicker
1122 whisker was always Caudal. Right, Peak induced contact pressure in the upper middle zone for
1123 identical 300- μ m whiskers with or without the intrinsic muscle element added to the model.

1124

1125

1126



A**Caudal Deflection****Rostral Deflection****B****Displacement****Change in angle****Change in curvature**